

Frequency Conversion of the 355 nm Nd:YAG Laser via Stimulated Raman Scattering in Hydrogen

J.A. Palero* and W.O. Garcia

Photonics Research Laboratory, National Institute of Physics
College of Science, University of the Philippines
Diliman, Quezon City 1101, Philippines
E-mail: jonathan@nip.upd.edu.ph

ABSTRACT

The third-harmonic 355 nm output of a pulsed Nd-YAG laser is converted into UV, VIS, and NIR laser light by stimulated Raman scattering in high pressure hydrogen gas. Laser lines in the 223 to 309 nm and 416 to 865 nm spectral regions are generated by anti-Stokes and Stokes Raman shifting, respectively. Experimental results on the energy output, conversion efficiencies, spectral profile, and temporal behavior of the various Stokes and anti-Stokes Raman laser lines are presented. The first and second Stokes shifted wavelength with wavelengths of 416 nm and 503 nm yielded a maximum energy conversion efficiency of 60.4% and 58.8% , respectively.

Key words: stimulated Raman scattering, Raman shifting, frequency conversion.

INTRODUCTION

Stimulated Raman scattering (SRS) is a powerful technique for shifting the wavelength of laser radiation into another spectral region. It is capable of simultaneously generating multiple laser lines ranging from vacuum ultraviolet (VUV) to far infrared (FIR). Compared to other frequency conversion methods, it is simple, economical, robust, and capable of high conversion efficiency. SRS has been used in a wide range of applications, such as generation of short laser pulses, time-gated low light level imaging, and lidar measurements.

In this work, the third harmonic 355 nm output of a pulsed Nd:YAG laser is shifted into the UV, VIS, and

NIR region of 223 to 865 nm through SRS in high pressure hydrogen gas. The energy, spectral profile, and temporal behavior of the Rayleigh and SRS lines are measured as a function of the 355 nm laser excitation energy and hydrogen gas pressure. SRS conversion efficiencies are calculated and presented.

Spontaneous and Stimulated Raman Scattering

A simplified diagram of the spontaneous Raman effect is illustrated in Fig. 1. An incident photon (ω_p) excites a molecule from the ground state to a virtual state. As the molecule relaxes to the first excited state, it emits a photon (ω_s) with a frequency lower than the incident photon. This frequency down-conversion process ($\omega_p > \omega_s$) is called Stokes shifting. If the incident photon (ω_p) is absorbed by a molecule initially in the first excited state, the emitted photon (ω_{AS}) will have a higher frequency as the molecule relaxes to the ground state. The up-conversion of the photon frequency ($\omega_p < \omega_{AS}$) is

*Corresponding author

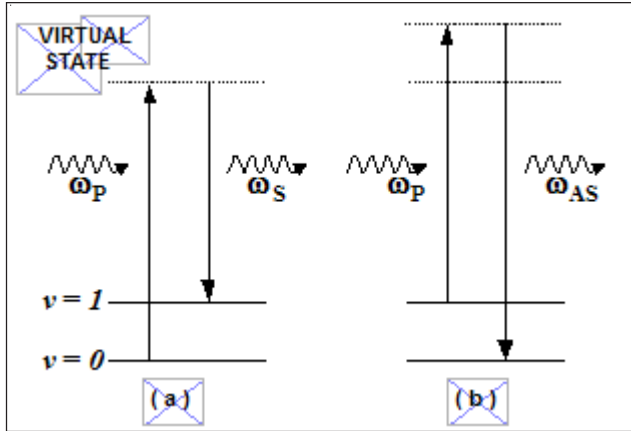


Fig. 1. A simplified diagram of the spontaneous Raman effect

referred to as anti-Stokes shifting. One of the characteristic parameters in this phenomenon is the energy difference between the first excited state and the ground state called the Raman frequency of the

medium. For hydrogen gas, this quantity is equal to 4155.25 cm^{-1} corresponding to the energy between the ground state and the first vibrational state.

At a sufficiently high incident photon flux, a process known as stimulated Raman scattering (SRS) can occur. It is a nonlinear optical process arising from the interaction of an intense laser beam with a Raman active medium such as CaCO_3 , SiCl_4 , CH_4 , and H_2 . The stimulated Raman scattering process is shown in Fig. 2. In Fig. 2a-c, a pump photon ω_p excites a molecule to the virtual state and interacts with a Stokes photon ω_s . Fig. 2d-f show the stimulated emission of an anti-Stokes photon by the interaction of an anti-Stokes photon and a molecule in a virtual state. In contrast to the incoherent radiation produced through the spontaneous Raman effect, SRS leads to the generation of coherent light that has the same wavelength and phase as the incident

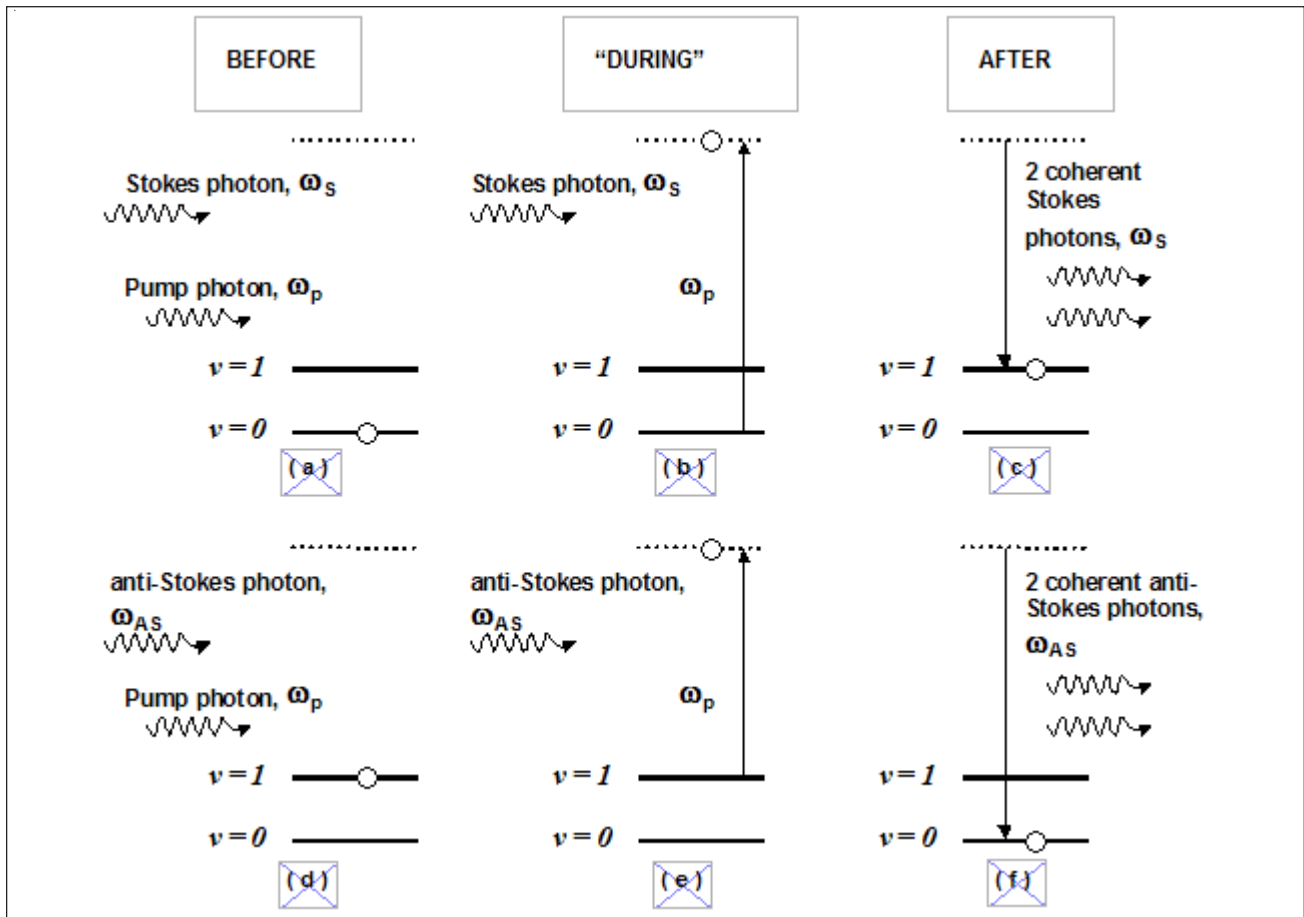


Fig. 2. The stimulated Raman scattering process.

photon. Furthermore, the SRS output is much more intense than the weakly scattered radiation from the spontaneous Raman effect.

If the intensity of the first Stokes-shifted frequency (S_1) is high enough, another SRS interaction can occur between S_1 and the medium. This process lead to the generation of a second Stokes-shifted frequency (S_2). Higher-order Stokes wavelengths are produced by this process known as SRS cascade. On the other hand, generation of higher order anti-Stokes wavelengths is also possible by a nonlinear process known as four-wave mixing (FWM). It involves the interaction of three waves to form a fourth wave. Fig. 3 shows the SRS cascade and FWM processes involved in the generation of Stokes and anti-Stokes wavelengths. Unlike the SRS process, the generation of radiation by FWM is sensitive to the phase mismatch between the wave vectors of the interacting waves. These leads to the low efficiency of the FWM process at high pressures where the phase mismatch is greatest. FWM also contribute to the generation of higher-order Stokes often to a greater extent than the SRS cascade. Table 1 shows the anti-Stokes and Stokes wavelengths generated by stimulated Raman scattering in hydrogen using a 355 nm laser excitation.

In the case of SRS in gases, the plane-wave steady-state Raman gain coefficient g_R is given by:

$$g_R = \frac{2 \lambda_s^2}{h c v_s} \frac{\Delta N}{\pi c \Delta v_R} \frac{d\delta}{d\Omega},$$

where λ_s is the Stokes wavelength (cm), v_s is the Stokes or Raman frequency (cm^{-1}), c is the speed of light (cm/s), h is Planck's constant (Js), ΔN is the difference in population between the initial and final states (cm^{-3}), Δv_R is the Raman linewidth (cm^{-1}), and $d\sigma/d\Omega$ is the differential cross section for Raman scattering (cm^2/sr). In the case of hydrogen, $\Delta v_R = 11.2/p + 1.58p$, where p is the gas pressure given in atm. An analysis

Table 1. Anti-Stokes and Stokes wavelengths generated by stimulated Raman scattering in hydrogen using a 355 nm laser excitation.

Raman Order	Wavelength
AS4	222.9
AS3	245.8
AS2	273.8
AS1	309.0
S1	415.9
S2	502.9
S3	635.9
S4	864.5

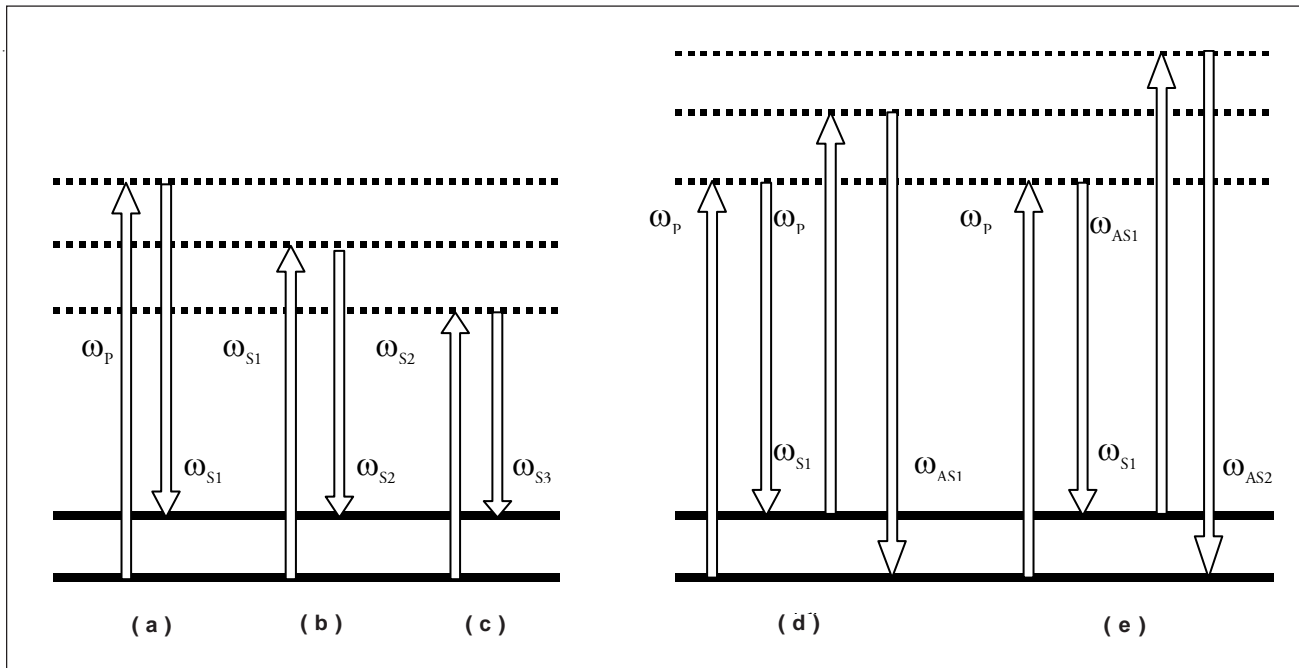


Fig. 3. The SRS cascade and FWM processes involved in the generation of Stokes and anti-Stokes wavelengths

of the gain coefficient as a function of pressure shows that it saturates for pressures greater than 20 atm. The Stokes intensity varies exponentially with the interaction length (z) as

$$I_S(z) = I_S(O) \exp (g_R I_L z)$$

where I_L and I_S are the incident laser intensity and the Stokes intensity. According to these equations, the Stokes intensity and the SRS conversion efficiency depend on laser beam intensity, laser beam geometry, and Raman active gas and its pressure.

EXPERIMENTAL SETUP & METHODOLOGY

Fig. 4 shows the schematic diagram of the Raman cell and the gas handling system. The Raman cell is constructed from stainless steel hollow cylinders that are welded together. Both ends of the cell are sealed with UV grade fused silica windows and o-rings. The cell is provided with inlet and outlet gas ports. A mechanical vacuum pump is used to evacuate the cell. Upon evacuation, ultra high purity hydrogen (99.9999% purity) is introduced into the cell from a gas cylinder through a gas regulator and shut-off valve. A mechanical pressure gauge monitors the hydrogen pressure.

A schematic diagram of the experimental setup is shown in Fig. 5. The laser is a Q-switched linearly polarized

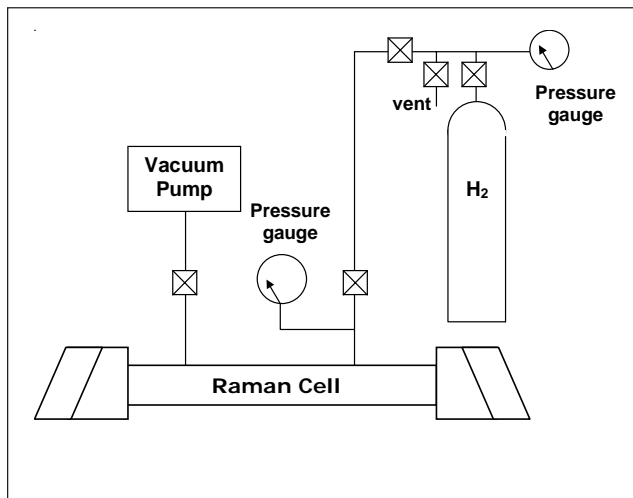


Fig. 4. The schematic diagram of the Raman cell and the gas handling system.

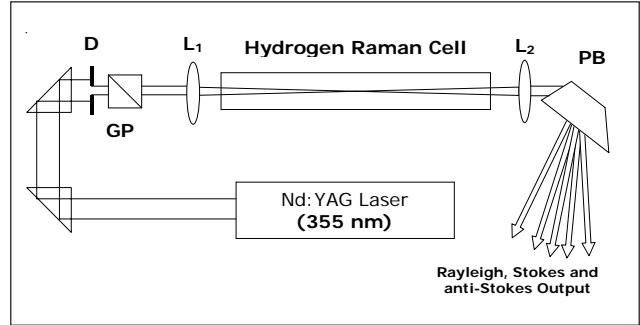


Fig. 5. Schematic diagram of the experimental setup

Nd:YAG laser (Spectra Physics GCR-230-10) which operates at 10 Hz pulse repetition rate, a wavelength of 1064 nm, and 5–8 ns (FWHM) pulse width. 355 nm output is obtained by the use of potassium dideuterium phosphate (KD*P) crystals.

The laser beam is passed through a diaphragm (D) set at an aperture of 1.5-mm diameter. A Glan laser polarizer (GP) is used to vary the laser pulse energy. The laser beam then is focused into a Raman cell using a 50 cm lens (L_1). A 30 cm lens (L_2) placed at the exit port of the cell is used to collimate the Raman output into a Pellin-broca prism (PB) for separation into the Rayleigh, SRS Stokes, and anti-Stokes components.

A pyroelectric detector (Molelectron J25HR) is used to measure the pulse energies of the 355 nm excitation laser, Rayleigh, SRS Stokes, and anti-Stokes lines. The spectral profile of the excitation, Rayleigh, SRS Stokes, and anti-Stokes lines are measured with a computer-controlled monochromator (SPEX 1000M). The temporal behavior is monitored with an ultra-fast biplanar phototube (Hamamatsu R1328U-5) and a 500 MHz digitizing oscilloscope.

RESULTS AND DISCUSSION

The spectral profile of the Raman output at a maximum input pump energy of 6.5 mJ and hydrogen pressure of 80 psi is shown in Fig. 6. There are eight Raman-shifted laser lines: four Stokes and four anti-Stokes, covering the ultraviolet to the near-infrared wavelength region. Spectral line-widths (FWHM) ranging from 0.02 nm to 0.08 nm are observed. Stokes lines are stronger than

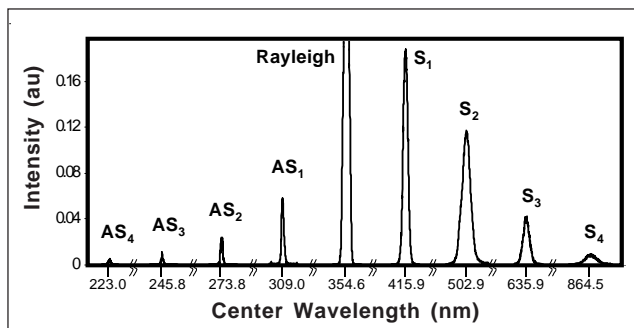


Fig. 6. The spectral profile of the Raman output at a maximum input pump energy of 6.5 mJ and hydrogen pressure of 80 psi

the anti-Stokes lines, and the intensity tends to weaken with increasing Raman order.

Fig. 7 shows the temporal behavior of the Raman output at different 355 nm laser excitation energy. The input laser pulse, which has a Gaussian profile, is truncated at half its maximum to show the temporal behavior of the scattered pulses more clearly. At an excitation energy of 2.27 mJ, generation of the first (S_1) and second Stokes (S_2) are observed. The 355 nm Rayleigh scattering has a lower energy than the input laser energy and a distortion in the pulse shape is observed due to the energy conversion into S_1 and S_2 . A delay time between the Rayleigh and S_1 is evident in the figure

due to the required pump threshold intensity to generate a Stokes pulse. S_2 also propagates with a time delay in respect to S_1 by the same reason, which also caused a distortion on the pulse shape of S_1 . The observed time delay in the generation of higher-order Stokes is a clear evidence of the SRS cascade process.

At an input laser energy of 4.45 mJ, the increase in intensity of S_1 and S_2 is accompanied by the generation of S_3 and AS_1 . Although S_2 increases in intensity, distortion in its pulse shape becomes apparent because of the onset of S_3 . The first anti-Stokes AS_1 is observed to propagate earlier than S_2 or S_3 which can be explained by the fact that anti-Stokes wavelengths are generated not by the SRS cascade but FWM. For instance, AS_1 is produced by the interaction of S_1 and two photons of the pump, and although it cannot propagate earlier than either S_1 or the Rayleigh, it may be generated earlier than the higher order Stokes.

An increase in intensity for all Raman-shifted pulses and the generation of a second anti-Stokes shifted pulse AS_2 are observed at 6.45 mJ of input laser energy. At this point, distortion of the Stokes pulses which may be due to the increased efficiency of FWM at high laser intensity becomes very apparent. The parasitic behavior of the anti-Stokes pulses with the Stokes is due to the

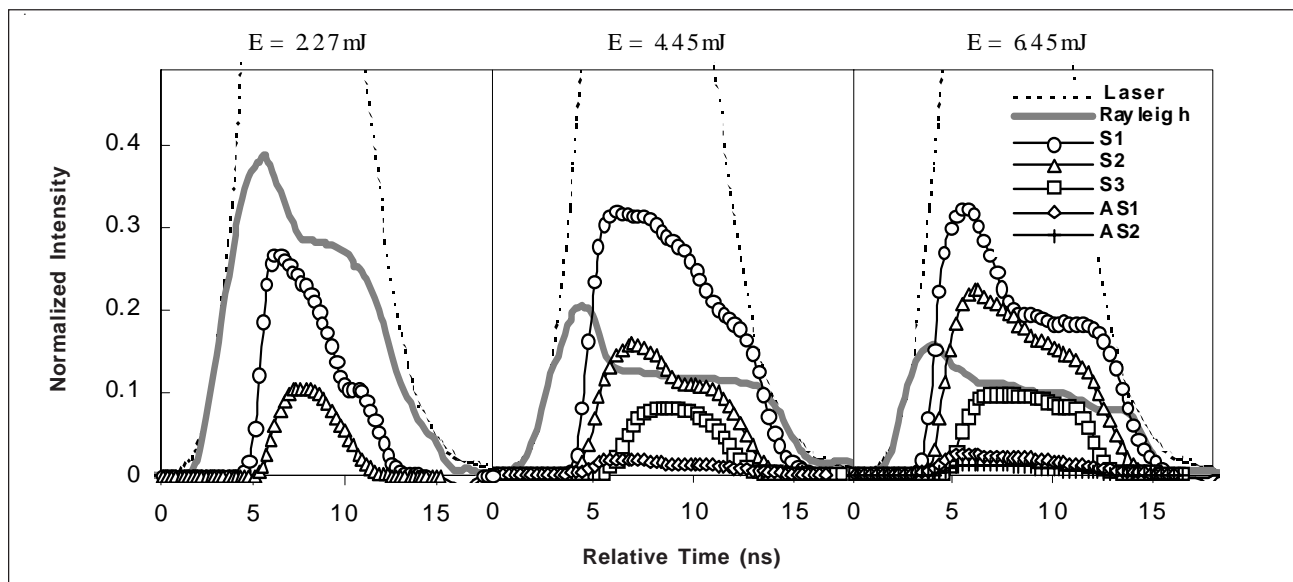


Fig. 7. The temporal behavior of the Raman output at different 355 nm laser excitation energy

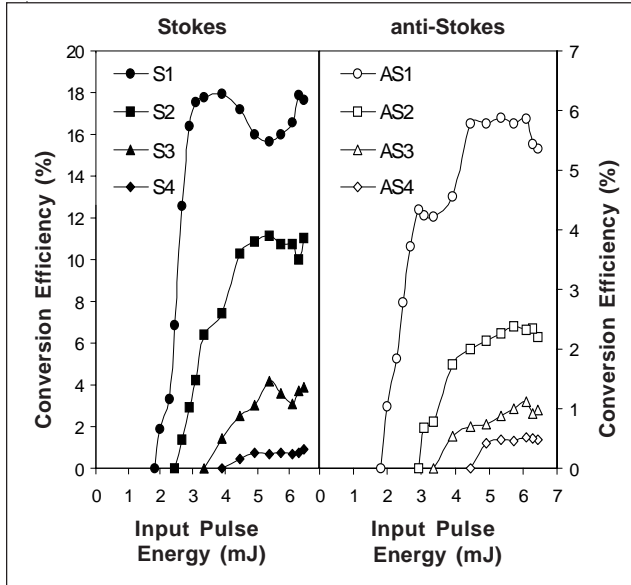


Fig. 8. Energy conversion efficiencies of the Stokes and anti-Stokes on the incident 355 nm laser energy at 80 psi hydrogen pressure

fact that generation of higher-order anti-Stokes through FWM is not restricted to the interaction of one set of waves. In fact, when n Stokes and anti-Stokes beams are present (total number, including the pump), there is a total of $(n-1)(n-2)/2$ distinct FWM processes among them.

Fig. 8 shows the energy conversion efficiencies of the Stokes and anti-Stokes on the incident 355 nm laser energy at a hydrogen pressure of 80 psi. The threshold for the generation of the first Stokes (S_1), S_2 , S_3 , and anti Stokes (AS_1) occur at 2.0 mJ, 2.7 mJ, 3.9 mJ, and 2.3 mJ, respectively.

The dependence of the Stokes and anti-Stokes conversion efficiencies with hydrogen pressure at 6.5 mJ of input laser energy is shown in Fig. 9. The conversion efficiency is defined as the ratio between the output energy and the laser input energy. The peak conversion efficiency of S_1 of 38% occurs at 300 psi. For S_2 , the peak conversion efficiency of 55% is attained at 500 psi. The conversion efficiency of the anti-Stokes reaches a maximum at around 80 psi. Anti-Stokes and higher-order Stokes are generated primarily by FWM processes at low pressures during which the phase mismatch of the interacting waves is minimum. At pressures greater than 150 psi, the phase mismatch is increased such that FWM is reduced. Fig. 10 shows

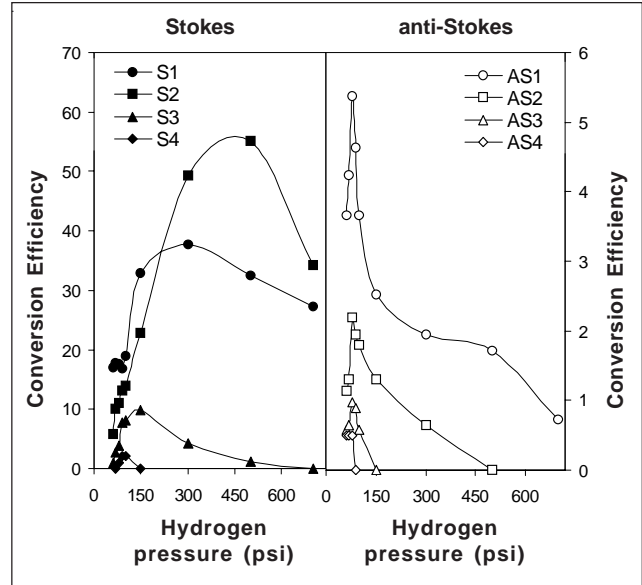


Fig. 9. The dependence of the Stokes and anti-Stokes conversion efficiencies with hydrogen pressure

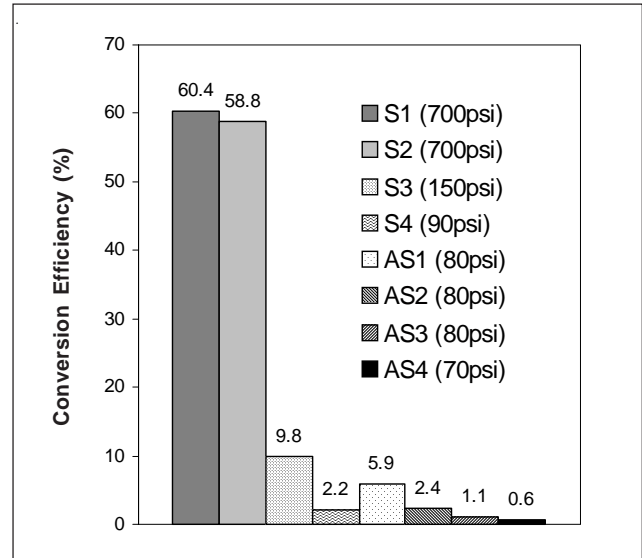


Fig. 10. Optimum energy conversion efficiencies of the Stokes and anti-Stokes

the optimum energy conversion efficiencies of the Stokes and anti-Stokes.

CONCLUSIONS

Stimulated Raman scattering in hydrogen is investigated as a method for generating laser radiation in the region of 223 to 865 nm (UV to NIR). A cascade process of

generation of the Raman components are observed from the temporal behavior of the output. The energy conversion efficiencies of the Stokes and anti-Stokes are observed to increase with increasing energy and to exhibit saturation. Anti-Stokes and higher-order Stokes are observed to have optimum conversion efficiencies at low pressures due to FWM generation while S_1 and S_2 are optimum at high pressures. Energy conversion efficiencies of 60%, 59%, 10%, and 2% are measured for S_1 , S_2 , S_3 , and S_4 Stokes wavelengths, respectively. On the other hand, 6%, 2%, 1%, and 0.6% conversion efficiencies are achieved for AS_1 , AS_2 , AS_3 , and AS_4 anti-Stokes wavelengths, respectively. These results are comparable to the results of Papayannis et al. (1998) who reported the generation of UV and VIS laser light in H_2 using a third harmonic 355 nm Nd:YAG laser pump with conversion efficiencies as high as 50% at the first Stokes shifted frequency.

ACKNOWLEDGMENTS

The authors acknowledge the assistance provided by Mr. Jose Omar S. Amistoso and Ms. Marian F. Baclayon, the support of the Philippine Department of Science and Technology through the Engineering and Science Education Project and the advise given by Dr. Caesar A. Saloma and Dr. Marlon H. Daza.

REFERENCES

- Carnuth, W. & T. Trickl, 1994. A powerful eyesafe aerosol lidar: Application of stimulated Raman backscattering of 1.06 mm radiation. *Rev. Sci. Instrum.* 65: 3324-3330.
- Chu, Z., U.N. Singh, & T.D. Wilkerson, 1991. Multiple Stokes wavelength generation in H_2 , D_2 , and CH_4 for lidar aerosol measurements. *Appl. Opt.* 30: 4350-4357.
- Duncan, M.D., R. Mahon, L.L. Tankersley, & J. Reintjes, 1992. Low-light-level, quantum-noise-limited amplification in a stimulated Raman amplifier. *J. Opt. Soc. Am. B.* 9: 2107-2121.
- Milton, M.J.T., G. Amcellet, A. Apituley, J. Bosenberg, W. Carnuth, F. Castagnoli, T. Trickl, H. Edner, L.

Stefanutti, T. Schaberl, A. Sunesson, & C. Weitkamp, 1998. Raman-shifted laser sources suitable for differential-absorption lidar measurements of ozone in the troposphere. *Appl. Phys. B.* 66: 105-113.

Papayannis, A.D., G.N. Tsirikas, & A.A. Serafetinides, 1998. Generation of UV and VIS laser light by stimulated Raman scattering in H_2 , D_2 , and H_2/He using a pulsed Nd:YAG laser at 355 nm. *Appl. Phys. B.* 67: 563-568.

Yamada, T., T. Nakata, & F. Kannari, 1995. Subnanosecond Pulse Generation in the VUV by Dual-wavelength Pumped Stimulated Rotational Raman Scattering. *IEEE J. Quantum Electron.* 31: 1274-1284.